









Water Resources Research®

RESEARCH ARTICLE

10.1029/2022WR032894

Flash Drought Onset and Development Mechanisms Captured With Soil Moisture and Vegetation Data Assimilation

Shahryar K. Ahmad^{1,2} , Sujay V. Kumar¹ , Timothy M. Lahmers^{1,3} , Shugong Wang^{1,2}, Pang-Wei Liu^{1,4}, Melissa L. Wrzesien^{1,3} , Rajat Bindlish¹, Augusto Getirana^{1,2} , Kim A. Locke^{1,3} , Thomas R. Holmes¹ , and Jason A. Otkin⁵ 

¹Hydrological Sciences Lab, NASA Goddard Space Flight Center (NASA GSFC), Greenbelt, MD, USA, ²Science Applications International Corporation, McLean, VA, USA, ³Earth System Science Interdisciplinary Center (ESSIC), University of Maryland, College Park, MD, USA, ⁴Science Systems and Applications, Inc., Lanham, MD, USA, ⁵University of Wisconsin-Madison, Madison, WI, USA

Key Points:

- Multivariate assimilation of remotely sensed vegetation and soil moisture helps characterize recent flash droughts in Northern Great Plains
- Heatwave-driven warm flash drought requires assimilating vegetation conditions to capture impact on transpiration during rapid development
- Use of soil moisture data is necessary to represent rapid drying of soils during the dry flash drought intensified by moisture deficit

Correspondence to:

S. K. Ahmad,
shahryarkhalique.ahmad@nasa.gov

Citation:

Ahmad, S. K., Kumar, S. V., Lahmers, T. M., Wang, S., Liu, P.-W., Wrzesien, M. L., et al. (2022). Flash drought onset and development mechanisms captured with soil moisture and vegetation data assimilation. *Water Resources Research*, 58, e2022WR032894. <https://doi.org/10.1029/2022WR032894>

Received 26 MAY 2022

Accepted 18 OCT 2022

Author Contributions:

Writing – review & editing: Jason A. Otkin

Abstract Flash droughts evolve and intensify rapidly under the influence of anomalous atmospheric conditions. In this study, we investigate the role of assimilating remotely sensed soil moisture (SM) and vegetation properties in capturing the evolution and impacts of two flash droughts in the Northern Great Plains. We find that during 2016 drought triggered by anomalously high temperatures and excessive evaporative demands, multivariate data assimilation (DA) of MODIS-derived leaf area index (LAI) and Soil Moisture Active Passive SM within Noah-Multiparameterization model helps capture elevated transpiration at onset. Assimilation of LAI particularly helped model the resulting rapid decline in SM during onset with as high as 10.0% steeper rate of decline compared to the simulation without any assimilation. Modeled-SM anomalies exhibit a 7.5% and 11.7% increase in similarity with Evaporative Stress Index (ESI) data and U.S. Drought Monitor (USDM) maps, respectively. In contrast, during 2017 flash drought driven by record-low precipitation during summers, SM assimilation resulted in largest rates of decline in rootzone SM, as large as 48.4% compared to results from no assimilation. Multivariate DA of SM and LAI results in 6.7% and 14.3% higher spatial similarity with ESI and USDM, respectively, and is necessary to model rapid intensification caused by anomalous precipitation deficits. This study elucidates the need to incorporate multiple observational constraints from remote sensing to effectively capture rapid onset rates, intensification, and severity of flash drought following different propagation mechanisms. This is fundamental for drought early detection to provide a wider window of response and implement efficient mitigation strategies.

Plain Language Summary A class of droughts called flash droughts develop rapidly under unusual weather conditions, often characterized by either warm temperatures or low precipitation or both. In this study, we employ the soil moisture (SM) and leaf area index (LAI) retrievals from the NASA Soil Moisture Active Passive mission and MODIS product, respectively, for characterizing the flash droughts of 2016 and 2017 in the Northern Great Plains. The results demonstrate that LAI observations, when assimilated within a land surface model, are effective in capturing high transpiration at the onset of 2016 drought driven by intense heat waves. The 2017 flash drought, however, was initiated by a precipitation deficit where information on SM is necessary to capture the rapid drying of soils. The modeled outputs not only capture the rapid drying of soil at the onset of droughts but are also spatially and temporally consistent with Evaporative Stress Index data and U.S. Drought Monitor maps. The study highlights the role of multivariate assimilation of remotely sensed vegetation and SM information to capture the rapid rates of onset and contrasting pathways of flash drought development.

1. Introduction

Human activities and climate change continue to exacerbate the occurrence and impact of extreme hydrologic events (Liu et al., 2021; Samaniego et al., 2018; Zhang et al., 2017). A detailed understanding of the evolution and mechanisms of hydrologic extremes, such as droughts, is paramount for managing and mitigating their impacts. Conventionally, a drought is considered a slowly developing climate phenomenon influenced by long-term changes to variables such as precipitation or evapotranspiration (ET; Svoboda et al., 2002; Wilhite & Glantz, 1985). As defined in Otkin et al. (2018), flash droughts involve both the unusually rapid rate of intensification (“flash”) and the condition of moisture limitation (“drought”). The rapid changes in water availability make flash droughts particularly challenging to predict and prepare for Lisonbee et al. (2021) and Woloszyn

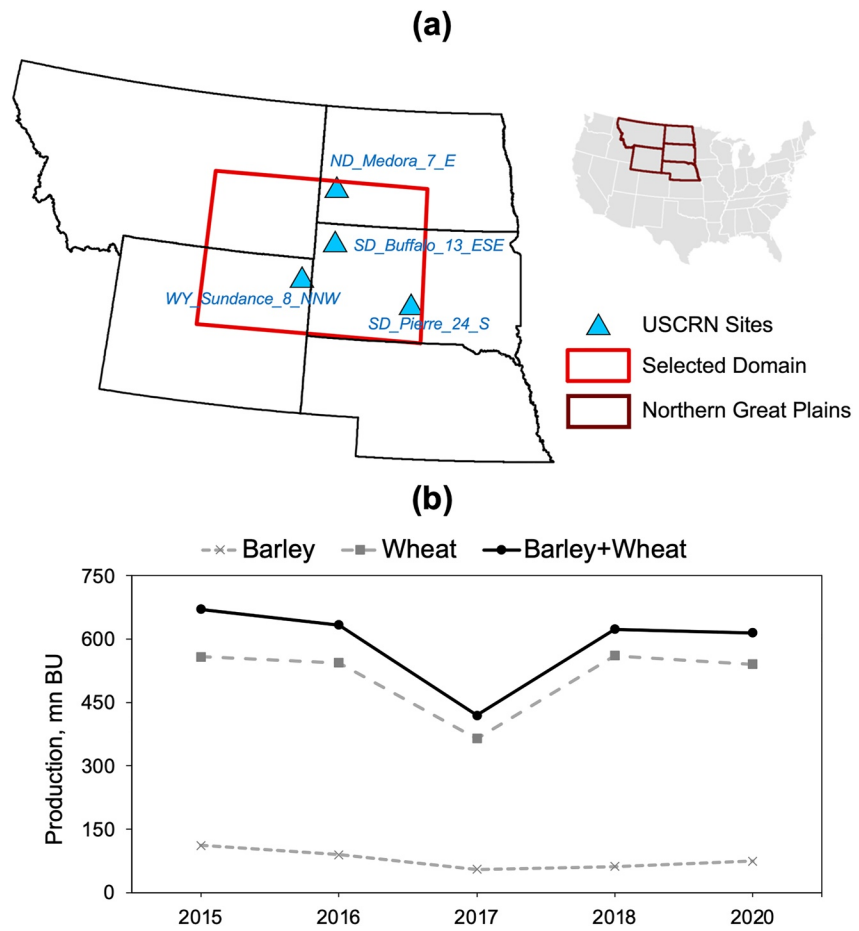


Figure 1. (a) Selected study domain (43° – 47° N, 108° – 100° W) in the Northern Great Plains and the selected U.S. Climate Reference Network (USCRN) sites for evaluating modeled soil moisture (SM). (b) Annual production of major crops planted in North Dakota and Montana showing the detrimental impact of the 2017 flash drought on growing season. Data from U.S. Department of Agriculture.

et al. (2021). Such rapidly intensifying events can be detrimental to vegetation health, especially if the dryness corresponds with a sensitive stage in crop development.

The rapid intensification of flash droughts can be triggered either by a heat wave, causing anomalously high air temperatures typically lasting two or more pentads, or as a response to unusually dry conditions caused by anomalously low precipitation. In the former, vegetation responds to excessive heat conditions and increased evaporative demands with a larger ET and reduced soil moisture (SM). SM here refers to overall moisture in the soil column unless qualified as root zone or surface SM. The SM decline continues even after the heat wave recedes accentuated by a lack of precipitation, which could have otherwise helped to reduce surface temperatures and replenish the SM. High temperatures can also cause stomatal closure, thereby reducing transpiration. The latter, primarily characterized by anomalous rainfall at the onset of the drought along with high ET demands, leads to anomalous rates of SM depletion and reduced transpiration, which exert stress on the vegetation. Thus, to distinguish between the droughts that not only differ in the triggers but also in the propagation mechanisms, here we use the terms “warm flash drought” and “dry flash drought” for droughts primarily involving temperature-driven and precipitation-driven intensification, respectively.

In the recent past, the U.S. Northern Great Plains region (Figure 1a) experienced two consecutive flash droughts in the years 2016 and 2017 (Gerken et al., 2018; He et al., 2019; Hoell et al., 2019; Kimball et al., 2019; Otkin et al., 2018). Both the droughts were classified as flash droughts mainly due to their rapid intensification in early summer. However, they were initiated and maintained by contrasting physical mechanisms. Due to their rapid onset, there was insufficient opportunity of early detection or to provide early warning to the agricultural

community to mitigate impending crop losses. For example, during the 2017 Northern Plains drought, neither the onset nor its severity was captured by NOAA's seasonal forecasts (Hoell et al., 2019). Instead, the prediction was for above-average precipitation during May–July 2017. Significant impacts included low crop production along with massive wildfires in the region (Jencso et al., 2019). Data from U.S. Department of Agriculture revealed the detrimental impact that 2017 flash drought had on annual production of major crops in the region (Figure 1b). In 2016, the U.S. Drought Monitor (USDM; Svoboda et al., 2002), an index that combines objective drought indicators with regional information, was late by several weeks in capturing the severity of vegetation stress, compared to ground-survey reports, during drought's intensification stage in June (Otkin et al., 2018).

Given the challenges in early detection and warning systems for flash droughts, it is imperative to explore whether the evolution of flash droughts driven by different physical mechanisms can be better characterized using a synergy of modeled, observed, and remotely sensed data. Several studies have focused on conventional drought monitoring by assimilating remote sensing observations of SM within hydrological models (Bolten et al., 2009; Kumar et al., 2014; Mladenova et al., 2019; Mozny et al., 2012; Xu et al., 2020; Yan et al., 2018). Data assimilation (DA) of vegetation conditions has also shown value in monitoring droughts and crop growth dynamics by improving ET and SM representation (Gavahi et al., 2020; Mocko et al., 2021; Nie et al., 2021).

Comparatively, flash droughts have received much less attention to advance their characterization. Existing efforts to monitor flash droughts have either used traditional indices over outputs from land surface models (LSMs) and climate models (Hobbins et al., 2016; Hoffman et al., 2021; Mishra et al., 2021; Otkin et al., 2013; Pendergrass et al., 2020; Yuan et al., 2019), or observations from remote sensing, in situ networks, or reanalysis products (Basara et al., 2019; Christian et al., 2019, 2021; Ford & Labosier, 2017; Mo & Lettenmaier, 2016; Otkin et al., 2019; Wang et al., 2016). For example, Otkin et al. (2013) use thermal infrared observations of land surface temperature. The recently proposed Flash Drought Stress Index (FDSI) employs SM retrievals from Soil Moisture Active Passive (SMAP) to measure the severity and rate of intensification of drought (Sehgal et al., 2021). The reliance on a single source of remote sensing information can be less effective in capturing rapidly developing flash drought mechanisms, particularly if they involve underlying processes not monitored by those measurements. For example, rapid soil drying during the onset of a moisture deficit-driven flash drought is more effectively captured if measurements of SM are employed. However, in a warm flash drought, where moisture depletes as a consequence of excessive heat and stress on vegetation, information on vegetation stress is necessary to capture the rapid evolution. Thus, multivariate observational constraints are needed to capture the underlying processes in a timely manner.

Due to orbital gaps and sensing limitations, remote sensing measurements typically have discontinuities in their coverage, which can be problematic for monitoring flash droughts due to their rapid nature of evolution. Also, the univariate observational constraint focus (either SM or vegetation) of many studies can be insufficient for the timely characterization of a flash drought. Therefore, techniques such as DA of multiple variables become important to develop spatially and temporally continuous coverage of relevant processes for effective flash drought characterization. This study presents a first-of-its-kind effort to use an advanced LSM and multiple remote sensing data sets together in a multivariate DA framework for timely and effective characterization of contrasting flash droughts.

Our objectives are twofold: (a) to evaluate the role of assimilating remotely sensed observations in capturing the onset and propagation of flash droughts at the earliest and (b) to use observational data to provide inferences on the appropriate processes relevant to flash droughts. Specifically, we focus on two flash droughts of 2016 and 2017 in the Northern Great Plains and model their propagation mechanisms by assimilating remotely sensed SM and leaf area index (LAI) into the Noah LSM with Multiparameterization options (Noah-MP; Niu et al., 2011). Although the 2016 and 2017 droughts were centered over slightly different parts of the Northern Great Plains, we select a common domain of study affected by droughts to provide a fair comparison of soil and vegetation dynamics across the two events (see Figure 1a). Multiple modeling experiments are designed, and model is validated against several reference data sets to demonstrate the utility of multiple observational constraints in representing the impacts of flash droughts on water cycle components. Using this modeling framework, we present a holistic assessment of the vegetation stresses and the response of vegetation to changes in soil conditions before and during the evolution of flash droughts. Given that one of the most distinctive and challenging features of flash droughts to model is their rapid rate of onset and intensification contributing to the “flash” aspect (Qing

et al., 2022), we also explore the utility of DA in capturing the rapid rate of decline in SM and vegetation conditions (LAI).

The rest of the paper is organized as follows. Section 2 provides a description of the LSM, data sets, and DA configuration. Section 3 presents the evolution and description of different aspects of the two flash droughts as captured by DA experiments, including an assessment of the modeled results. Finally, Section 4 presents the summary and key conclusions from this study.

2. Materials and Methods

2.1. LSM Configuration

The modeling framework uses Noah-MP LSM which augments the Noah LSM with improvements to the model structure, parameterization schemes for biophysical and hydrological processes, and snow skin temperature representations (Niu et al., 2011; Yang et al., 2011). The Noah-MP LSM (Version 4.0.1) and DA schemes are implemented within the open-source NASA Land Information System (LIS) framework (Kumar et al., 2006; <https://github.com/NASA-LIS/LISF/>). Noah-MP LSM is particularly chosen because of the flexibility to use different parameterization schemes. In particular, the use of a dynamic vegetation phenology scheme in Noah-MP to represent vegetation growth (Niu et al., 2011; Yang et al., 2011) allows for assimilating observations of vegetation conditions such as LAI. Noah-MP is configured to simulate four soil layers with individual layer thicknesses of 0.1, 0.3, 0.6, and 1.0 m resulting in a total of 2.0 m of soil depth from the surface. Quantitative analysis is performed over the drought-affected region of Northern Great Plains (43°–47°N, 108°–100°W) during the two flash droughts (Figure 1a). A spatial resolution of 10 km with a 15-min time step is chosen for the simulations. All model runs are performed over the period of April 2015 to December 2020 (the overlap period across all the data sets).

2.2. Data Sets

Noah-MP LSM is forced with precipitation from the Integrated Multi-satellitE Retrievals for Global Precipitation Measurement (IMERG; Huffman et al., 2015) post-time Final Run product, Version 06B. Other meteorological forcing fields of 2-m air temperature, 2-m specific humidity, 10-m wind speed, surface pressure, and incoming shortwave (SW) and longwave (LW) radiation are obtained from the Modern-Era Retrospective Analysis for Research and Applications, Version 2 (MERRA-2; Gelaro et al., 2017).

MODIS LAI and SMAP SM observations are used for DA within the Noah-MP LSM. The LAI in the LAI-DA integrations is derived from the level 4, 500-m resolution, 8-day composite MCD15A2H Version 6 Moderate Resolution Imaging Spectroradiometer (MODIS) product. The product algorithm chooses the best pixel available from all the acquisitions of MODIS sensors located on the Terra and Aqua satellites (Myneni et al., 2015). The 500-m resolution LAI data are aggregated to the 10 km model resolution to be integrated within the LSM. Only the “good quality” data values not flagged for cloud contamination, detector signal problems, and algorithm saturation issues are used for DA.

SM is obtained from SMAP mission, downscaled using the Thermal Hydraulic disaggregation of Soil Moisture (THySM) algorithm (Liu et al., 2021, 2022). SMAP satellite (Entekhabi et al., 2010), uses L-band microwave sensor to provide surface SM at the top 5 cm soil layer with 36-km spatial resolution. The THySM algorithm incorporates ancillary data sets at high spatial resolution based on thermal inertia theory and water retention curves to improve the spatiotemporal resolution of SMAP and outputs SM fields at 1 km. The downscaling approach is based on the principle that dry soil drives stronger heat transport, resulting in higher temperature variation during a day while, wet soil results in smaller temperature changes (Liu et al., 2021).

2.3. DA Configuration

Similar to previous studies (Kumar et al., 2009, 2014, 2019; Liu et al., 2013, 2015; Yin et al., 2015), a one-dimensional ensemble Kalman Filter (EnKF; Reichle et al., 2002) is employed here to assimilate SM and LAI retrievals into the Noah-MP LSM. Consistent with Kumar et al. (2019), an ensemble size of 20 is used for the DA and perturbations are applied to meteorological and model prognostic fields to maintain ensemble spreads

representing the uncertainty in model estimates. EnKF uses ensemble members to quantify the covariances and as the observation becomes available, the state vector of each ensemble member is propagated forward in time. The general form of the analysis step can be written as

$$x_k^+ = x_k^- + K_k(y_k - H_k x_k^-) \quad (1)$$

where x_k^+ is the posterior state vector after the update, x_k^- is the prior model state vector, y_k is the observation vector, and H_k is the observation operator that relates the model states to the observations. The subscript k indicates time and matrix K_k is the gain matrix, which essentially represents the weighting factor to determine the degree to which the model forecast is adjusted toward the observation.

The setup for assimilating LAI and SM observations within the LSM involves introducing small perturbations to several meteorological forcing inputs (downward SW radiation, downward LW radiation, and precipitation) and modeled LAI and SM states at each grid point. A configuration similar to Kumar et al. (2021) is employed where multiplicative perturbations are applied with standard deviations of 0.3 and 0.5 to precipitation (P) and downward SW radiation, respectively, and additive perturbation with standard deviations of 50 W/m² to downward LW radiation. Cross-correlations (ρ) to perturbations between each of forcing fields are also included, where $\rho(\text{SW}, \text{P}) = -0.8$, $\rho(\text{SW}, \text{LW}) = -0.5$, and $\rho(\text{LW}, \text{P}) = 0.5$. Further, a uniform observation error standard deviation of 0.05 for MODIS-derived LAI retrievals is used in the LAI-DA configuration following Kumar et al. (2021). For SM-DA configuration, however, an observation error standard deviation of 0.04 m³/m³ is used which matches the satellite retrieval accuracy (Xu et al., 2020) and follows Kumar et al. (2019). The Multi-DA configuration, with similar perturbations, jointly assimilated the SM and LAI observations at their respective local overpass times. Four experiments are conducted to model flash drought progression. These include a baseline open loop (OL) run of Noah-MP without any assimilation, and three DA runs where SM and LAI are assimilated either independently (called SM-DA and LAI-DA, respectively) or simultaneously (Multi-DA).

2.4. Evaluation Framework

For a quantitative analysis and assessment of the LSM outputs, we first calculate daily deviations (anomalies) from the mean across 2015–2020 for modeled root zone SM (RZSM), LAI, and transpiration. The respective daily standard deviations across all the years under consideration are also calculated. The anomalies are then normalized with those standard deviations to derive standardized anomalies, which facilitate comparison across the regions and data sets due to a common range of variation.

RZSM anomalies are compared against data sets of Evaporative Stress Index (ESI) at 4-km resolution. ESI describes temporal anomalies in ET which includes the loss of water via evaporation from soil and plant surfaces and via transpiration through plant leaves. ESI is developed with the thermal remote sensing-based Atmosphere-Land Exchange Inverse (ALEXI) surface energy balance model (Anderson et al., 2007, 2011). Negative ESI values show below normal ET rates, indicating vegetation that is stressed due to inadequate SM.

We compare 1-month composite ESI at weekly intervals with the weekly averaged RZSM anomalies using Pearson's correlation (R) and Mutual Information (MI) score. The MI score is a nonparametric generalization of the Pearson's R that can handle nonlinear relationships between non-Gaussian variables (Tuttle & Salvucci, 2014). It measures the mutual dependence of two random variables by quantifying the dependence between the joint distribution of the variables when they do not follow Gaussian distribution. MI for two variables, X and Y , is defined as

$$\text{MI}(X; Y) = \sum_{y \in Y} \sum_{x \in X} p(x, y) \log \left[\frac{p(x, y)}{p(x)p(y)} \right] \quad (2)$$

where $p(x)$ and $p(y)$ are the marginal probability distribution functions of X and Y , respectively, and $p(x, y)$ is the joint probability distribution function of those variables. In our case, the two variables are RZSM and ESI anomalies. The metric is implemented in the scikit-learn package as *mutual_info_score*.

Another aspect of evaluation is the spatial consistency of the modeled RZSM with drought categories from USDM drought maps. Structural Similarity Index (SSIM) is used to measure perceived similarity in the structure of two images and compare the local patterns of normalized pixel intensities (Wang et al., 2004). SSIM has

also been used to evaluate modeled ET by Walker et al. (2019). The index combines the luminance and contrast between two images and normalizes the product with the standard deviation to perform the structural comparison. SSIM for two image windows, x and y , is calculated as

$$\text{SSIM}(x, y) = \frac{(2\mu_x\mu_y + c_1)(2\sigma_{xy} + c_2)}{(\mu_x^2 + \mu_y^2 + c_1)(\sigma_x^2 + \sigma_y^2 + c_2)} \quad (3)$$

where μ_x and μ_y are the averages of x and y , σ_x and σ_y are variance of x and y , and σ_{xy} is the covariance of the two windows. Further, $c_1 = (k_1L)^2$ and $c_2 = (k_2L)^2$ are two variables that stability the division operation, L is dynamic range of pixel values, and k_1 and k_2 are fixed as 0.01 and 0.03, respectively. Monthly averages of RZSM anomalies over May-Aug are compared with the drought categories D1–D4 from the USDM maps for the respective months.

Because modeled RZSM anomalies are continuous in nature unlike the discretized USDM drought category maps, we also used F1-score as another measure of spatial consistency between the two data sets. F1-score is the harmonic mean of two other metrics, Precision and Recall scores. Precision is a ratio of the number of true positives (TP) and the sum of TP and false positives (FP), while recall is the number of TP divided by the sum of TP and false negatives (FN).

$$\text{Precision} = \frac{\text{TP}}{\text{TP} + \text{FP}} \quad (4a)$$

$$\text{Recall} = \frac{\text{TP}}{\text{TP} + \text{FN}} \quad (4b)$$

$$\text{F1} = \frac{2 * \text{Precision} * \text{Recall}}{\text{Precision} + \text{Recall}} \quad (4c)$$

In our case, the monthly RZSM anomalies are classified into discrete classes using thresholds of $(-0.25, -0.5, -0.75, -1)$ which are then compared with the respective drought categories. A more involved comparison with USDM classes will require calculation of SM percentiles which was not feasible due to limited availability of SMAP data used in assimilation. Finally, modeled surface SM (nonnormalized) is also evaluated against observations from U.S. Climate Reference Network (USCRN) sites. Four USCRN sites were selected in Northern Great Plains (Figure 1a) and the RMSE and bias for each station is compared with Noah-MP modeled surface SM.

3. Results and Discussion

This section describes the results from the modeling and DA integrations. Given the rapid development aspect of flash droughts, we conduct all the analysis at a daily time scale. However, spatial maps of drought progression are shown at a monthly time scale for the sake of brevity.

3.1. Flash Drought Onset

The onset of flash droughts is triggered by either anomalously low precipitation causing unusually dry conditions or anomalously high temperatures resulting in heat waves or a combination of both. Here, we first characterize the processes that led to the onset of each drought event over the selected domain in Northern Great Plains (see Figure 1a for domain). Figure 2 shows the temporal evolution of domain-averaged precipitation and near surface air-temperature anomalies from the model runs during March–September of 2016 and 2017, along with the domain-averaged ESI. The daily precipitation and near surface air-temperature anomalies are normalized with standard deviation using the multiyear mean over 2015–2020 and accumulated as moving average at weekly time scales to smooth out the daily variability. Negative ESI anomalies convey deteriorating vegetation conditions.

Figure 3a shows the spatial progression of standardized anomalies of precipitation and near surface air temperature for 2016 flash drought. Precipitation events brought wetter-than-normal conditions in March particularly across Wyoming and later in April across most of the states in the Northern Plains. High temperatures dominated

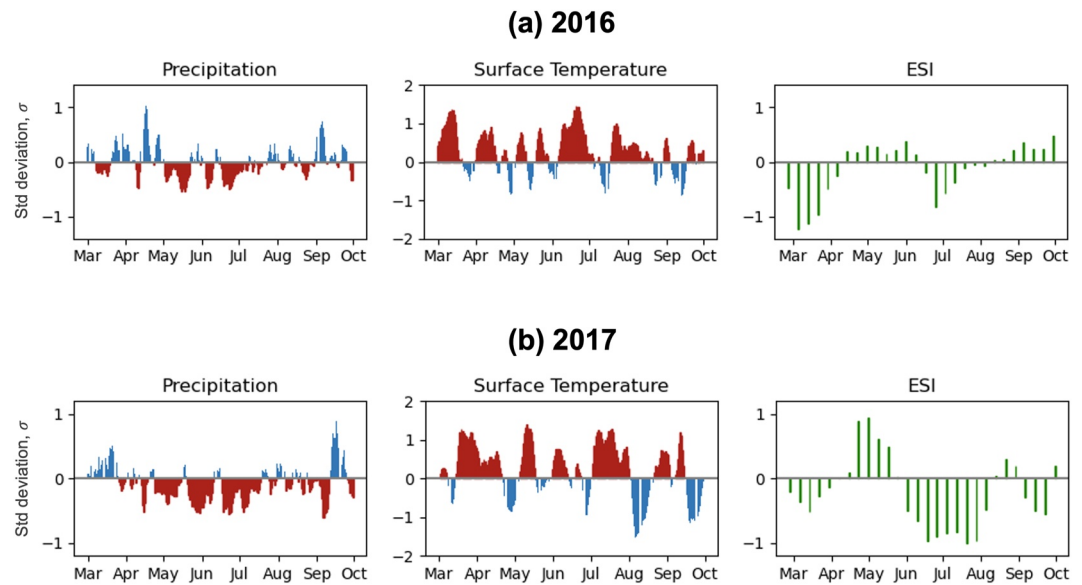


Figure 2. Standardized anomalies of precipitation, near surface air temperature, and Evaporative Stress Index (ESI) averaged over the selected domain during the flash droughts of (a) 2016 and (b) 2017.

the drought onset and intensification in May and June, leading to subsequent deteriorations in SM and vegetation conditions, as evidenced by large negative ESI anomalies (rightmost panel in Figure 2a).

In contrast, a key driver of the 2017 drought was record-low precipitation during May–July, which is usually the wettest climatological season in the region (Figure 3b). Dry soil conditions appeared simultaneously with warm temperatures in May, leading to the intensification of flash drought in the following summer months (Figure 2b). Negative ESI anomalies again capture the impact of anomalously dry soils during drought intensification in

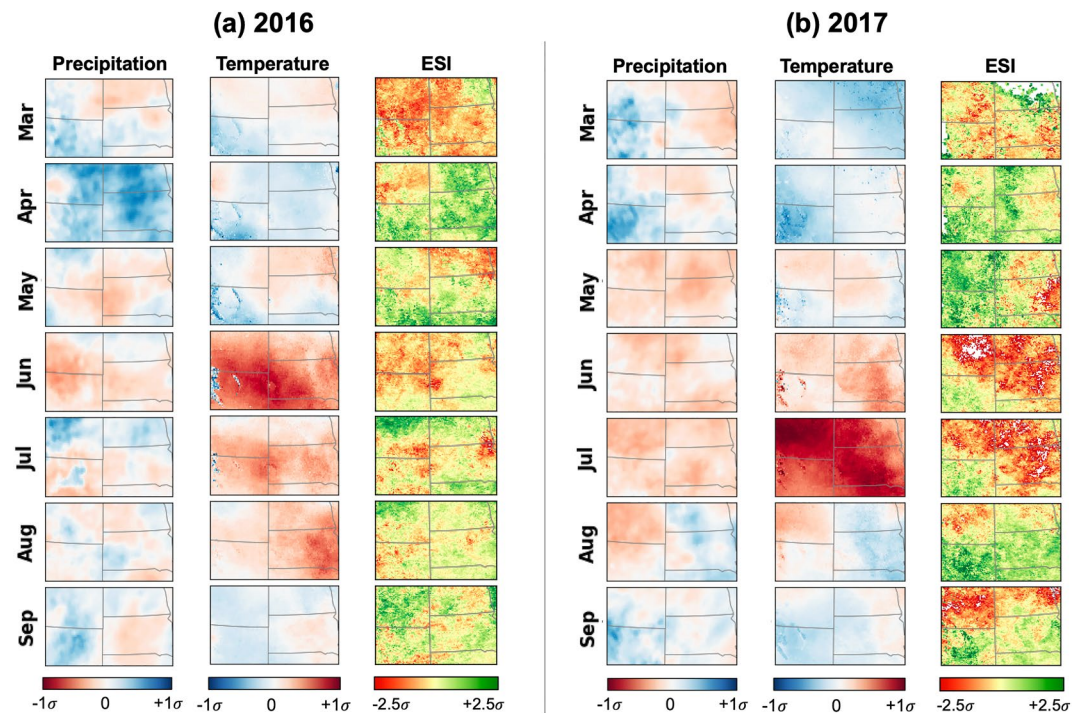


Figure 3. Spatial progression of the standardized anomalies of precipitation, near surface air temperature, and Evaporative Stress Index (ESI) (in units of standard deviation) during the flash droughts of (a) 2016 and (b) 2017.

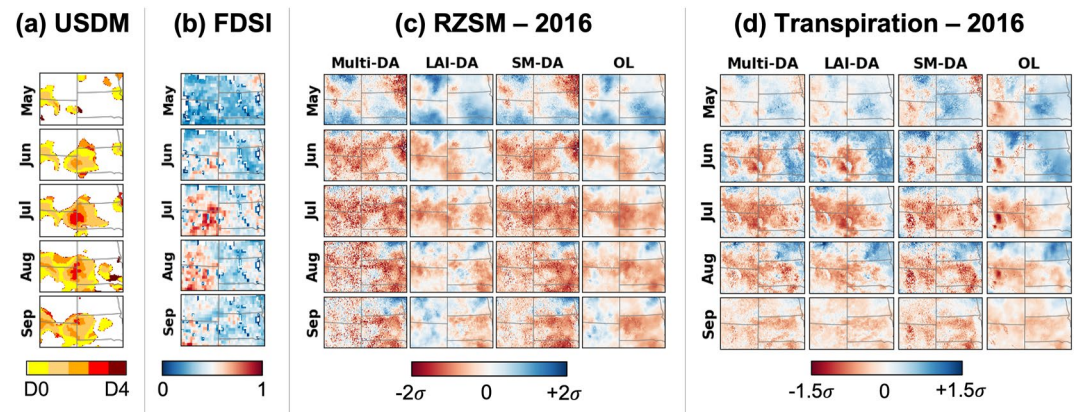


Figure 4. Spatial progression (upper panel) of the flash drought of 2016 from (a) U.S. Drought Monitor (USDM; monthly median); (b) monthly averaged Flash Drought Stress Index (FDSI); and using the monthly standardized anomalies (in standard deviations) of (c) root zone soil moisture (RZSM) and (d) transpiration modeled from different land surface model (LSM) configurations. Areas shown are larger than the selected domain of Figure 1a to show the surrounding context of droughts.

June and July. Given that ESI is a land surface temperature-based product, severity of the heat wave-driven 2016 drought is more pronounced in the ESI anomalies during the onset, compared to the 2017 drought. The contrasting drivers in 2016 and 2017 caused the flash droughts to progress differently.

3.2. Impact of DA on Characterizing Warm Flash Drought of 2016

Figure 4 shows the spatial progression of 2016 drought in terms of the standardized anomalies in RZSM and transpiration along with the median of weekly USDM maps produced each month. Comparisons are at monthly time steps between the DA configurations (LAI-DA, SM-DA, and Multi-DA) and OL simulation. The intense heatwave at the onset in March 2016 caused vegetation to respond with increased transpiration followed by a resulting decline in RZSM. Subsequent precipitation events in April led to wetter conditions, captured by OL and all the DA runs with positive RZSM anomalies across most of the domain (Figure 4c, top row).

The impact of DA is most apparent during the peak intensification of flash drought during June and July when the return of warmer-than-normal temperatures along with persistent dry conditions significantly stressed the vegetation (see Figure 3a). The transpiration in June exhibited large negative anomalies when modeled with LAI-DA that were otherwise not captured by OL or SM-DA simulation (Figure 4d). Spatial patterns in transpiration compared better with hotspots from USDM maps on assimilating LAI information, though USDM had some issues in capturing the drought severity for this case, as noted earlier. Once vegetation stress takes effect, observations of SMAP SM are useful to model the resulting deterioration in RZSM during June and July captured by the relatively larger negative anomalies in Multi-DA and SM-DA simulations. Multi-DA thus combines the information from both LAI and SM to effectively model the drought intensification when USDM recorded a two-category increase in drought severity (Figure 4a). Precipitation in August and September helped improve the conditions in the region with largest improvements in the Dakotas as evidenced by subsequently less negative RZSM and transpiration anomalies across the LSM runs. The RZSM anomalies are also compared with FDSI over the drought period as shown in Figure 4b. The comparisons reveal that, although FDSI captures the drought hotspots in July that are spatiotemporally consistent with USDM categories, once the vegetation stress takes effect, resulting deterioration of RZSM in the eastern parts of the domain is generally underestimated in FDSI. Assimilating MODIS LAI and SMAP SM helps model those stresses captured by the relatively large negative anomalies in the Multi-DA simulation in the eastern parts.

The daily variation of standardized anomalies of LAI, RZSM, and transpiration, averaged over the selected domain, is shown in Figure 5 explaining the temporal influence of DA experiments in capturing drought progression. The month of April 2016 received abundant precipitation which eliminated the abnormally dry soil conditions and reduced stress on the vegetation (as shown by large positive ESI anomalies in April in Figure 3a). While MODIS LAI observations are available only every 8-day, assimilating SM observations (Multi-DA and

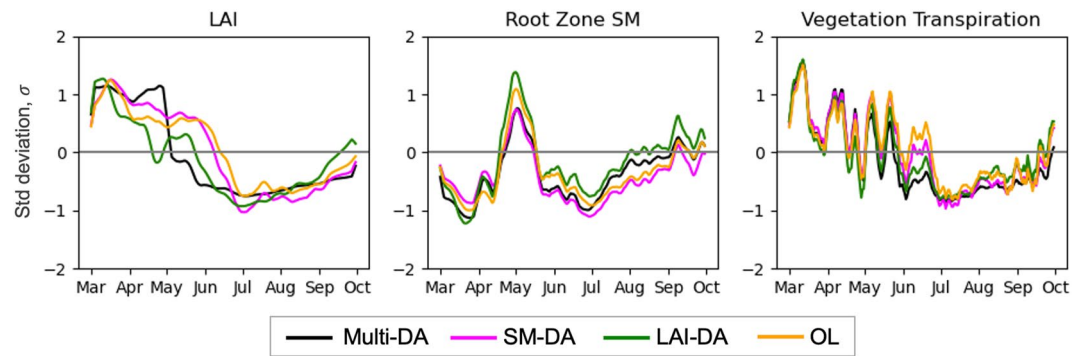


Figure 5. Temporal progression of leaf area index (LAI), root zone soil moisture (RZSM), and transpiration anomalies, averaged over the selected domain for 2016 flash drought.

SM-DA simulations) results in increased LAI anomalies in April (compared to LAI-DA), reflecting the apparent reduced stress on vegetation. This also caused Multi-DA to have larger positive LAI anomalies, closer to those modeled from SM-DA simulations during April. Subsequent drier conditions in May caused a sharp decline in LAI modeled with Multi-DA relative to the SM-DA and OL simulations, capturing the increasing vegetation stress (Figure 5, leftmost panel). Another factor that aggravated the vegetation condition was the occurrence of several days of freezing temperatures in mid-May (see Figure 2a). Though lower temperatures during May are not unusual in this region, the severity and persistence of the cold temperatures were unusual, termed as “hard freeze” by Otkin et al. (2018), resulting in a less-resilient vegetation. With the return of above normal temperatures, stressed vegetation continued to result in large negative RZSM anomalies over the drought intensification period.

Changes in LAI have a direct impact on the water cycle components. Decreased LAI leads to reduced canopy shading, increased net radiation, and a resulting decrease in SM. Conditions improved gradually post-June with near-normal temperatures and rainfall, but LAI anomalies remained negative. This could be attributed to the impacted development cycle of most crops and rangelands during summers and the longer-term impacts of heightened vegetation stress. The assimilation of MODIS-derived LAI is essential to capture the response of vegetation to the 2016 drought initialized by heat waves and intensified by dry conditions.

3.3. Impact of DA on Characterizing Dry Flash Drought of 2017

The 2017 flash drought followed a contrasting pathway primarily due to anomalously low precipitation during the climatologically wet season of May-July, leading to a peak drought intensity in July. Figures 6c and 6d show the spatial progression in RZSM and transpiration anomalies as the drought developed. Prior to the onset in March, RZSM was adequate across most of the Northern Great Plains due to early precipitation. Wet soil conditions in

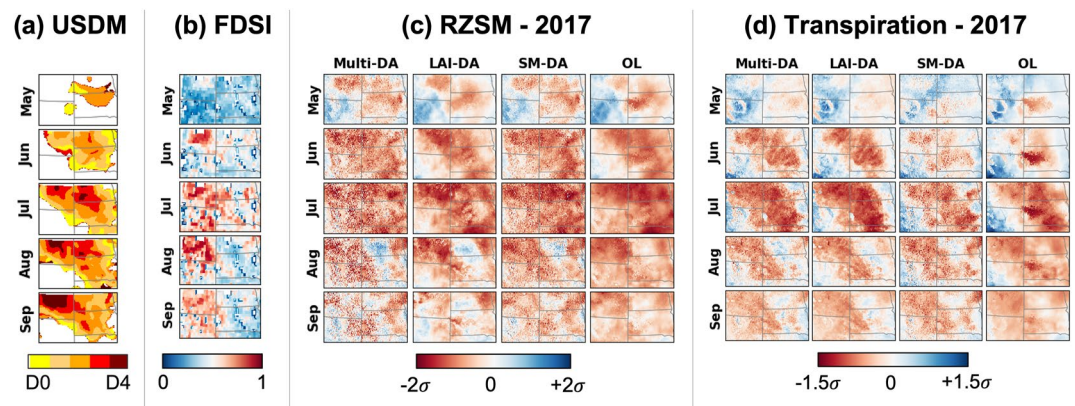


Figure 6. Same as Figure 4, but for the flash drought of 2017. Areas shown are larger than the selected domain of Figure 1a to show the surrounding context of droughts.

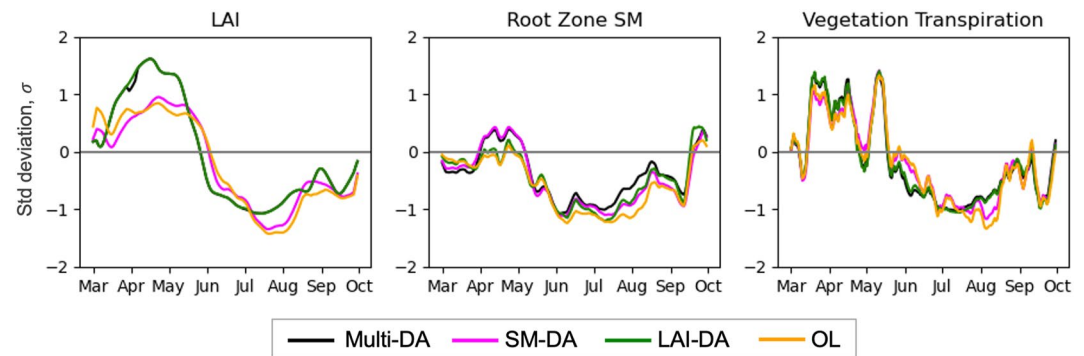


Figure 7. Same as Figure 5, but for the flash drought of 2017.

May (Figure 6c, top row) began to experience rapid decline during an anomalously dry period in May–July. The RZSM anomalies from SM-DA and Multi-DA simulations are spatially more consistent with USDM drought patterns (see Section 3.5 for a quantitative evaluation) and detect early signals of rapid drought intensification in June (Figures 6a and 6c). Assimilating information on SM helps resolve the rapid rate of change in moisture availability. The vegetation stress during onset, a consequence of the moisture stress for this drought event, is overestimated in the integrations that only incorporate LAI. On the other hand, during the late summer months (August–September), LAI-DA modeled outputs underestimate drought severity, whereas SM-DA results in relatively more stressed vegetation conditions. The rapid drawdown in moisture is also captured by FDSI leading to larger drought severity around the USDM hotspots during the peak drought months of July and August (Figure 6b). However, the severity is clearly underestimated in the eastern part of the domain. Again, our DA experiments, by incorporating both the vegetation and SM conditions, help capture the additional stress brought by vegetation response to result in rapid moisture drawdown for this drought event.

Although assimilation of SM observations in SM-DA and Multi-DA simulations helps capture the large negative anomalies across the region during the peak intensification period, particularly for the dry flash drought of 2017, resulting anomalies exhibit noisier patterns compared to LAI-DA or OL. DA setup applies a number of LSM-based quality control procedures to specify when and where observations should be assimilated, in addition to the screening applied to the observations based on quality flags within SM retrievals. SM observations are excluded for assimilation for being at the edge of the swath, near water bodies, and when impacted by dense vegetation, precipitation, frozen ground, snow cover, or radio frequency interference based on the information provided in the SM retrievals (Kumar et al., 2014). Comparatively, the observation screening procedure within LAI-DA is simpler, primarily based on the observation quality flags only (Kumar et al., 2019). These procedures in the SM assimilation, while essential, may lead to differing assimilation instances across neighboring pixels and ensemble members contributing to the noisy features, particularly at high resolutions.

Temporal variations of the drought indicators of LAI, RZSM, and transpiration are shown in Figure 7. SM-DA and Multi-DA capture the positive RZSM anomalies at the onset (April–May) while OL and LAI-DA are unable to model this response (Figure 7, middle panel), as the primary drought signal is influenced by SM. The negative LAI anomalies during the summer months (Figure 7, left most panel) are the result of overstressed vegetation in response to increased evaporative demand and depleted SM. Assimilating SMAP SM thus helped in modeling the rapid decline in moisture that caused the vegetation to respond with reduced transpiration. Because vegetation stress is not the primary driver of drought onset or intensification in 2017, assimilating SM observations do not have any significant impact on the modeled vegetation response and Multi-DA mostly follows LAI-DA simulation in the LAI and transpiration anomalies.

The following sections describe the improvement from LSM and DA to the representation of flash drought onset and intensification and the subsequent drought severity.

3.4. Multivariate DA Captures Drought “Flashiness” at the Onset

One of the distinctive features of flash drought that separates it from conventional long-term droughts is its rapid rate of intensification contributing to the “flash” aspect (Otkin et al., 2018; Qing et al., 2022). Here, we explore

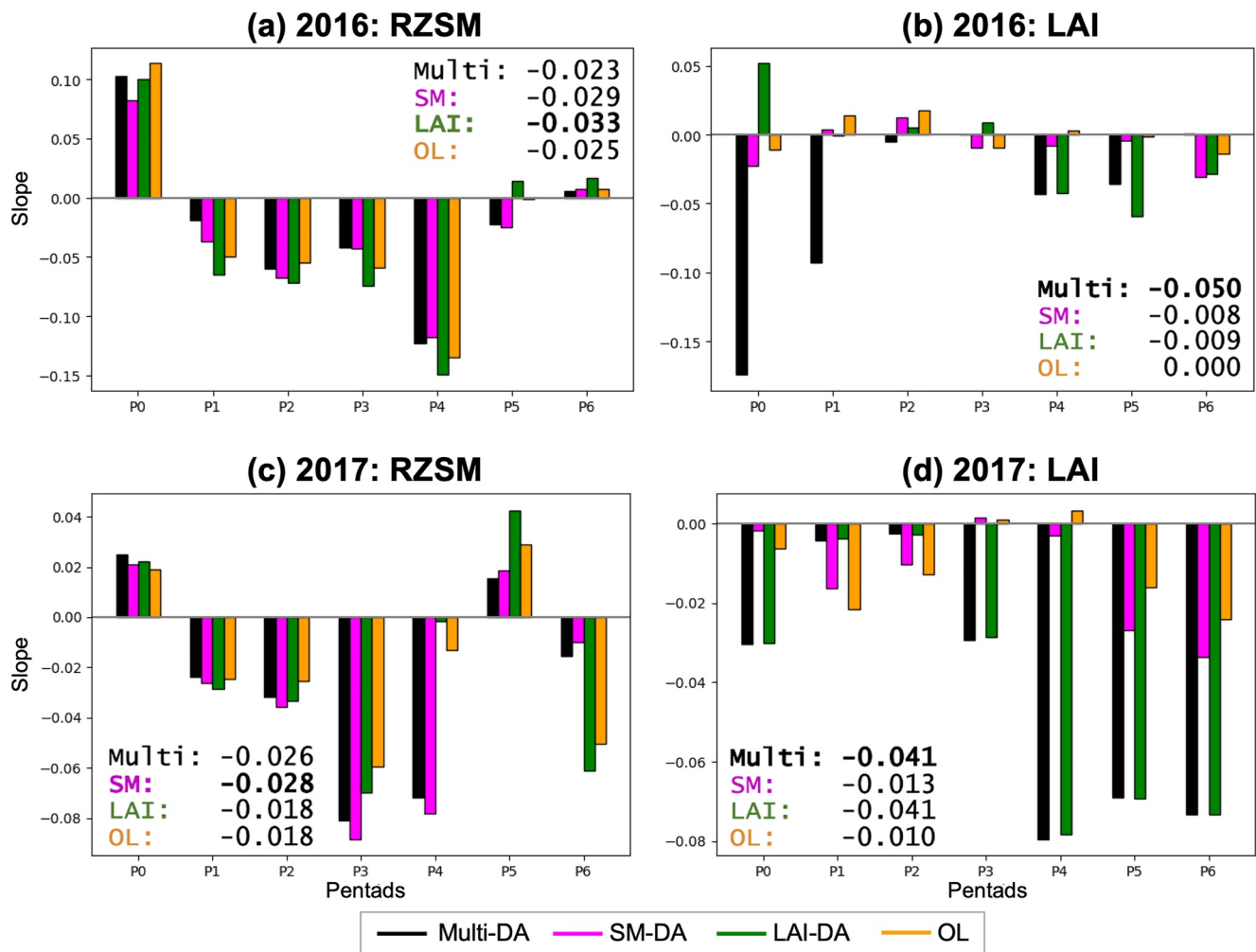


Figure 8. Average slopes for (a) root zone soil moisture (RZSM) and (b) leaf area index (LAI) over seven pentads, where pentad zero corresponds to the last pentad with positive slope of RZSM preceding the decline to lowest pentad slope, over the 2016 flash drought. Plots (c) and (d) show the same for 2017 flash drought. Annotation on the plots summarize average slope over the seven pentads for each model configuration, bold font shows the one with minimum slope.

the utility of assimilation in capturing the rapid rate of onset and intensification of flash droughts. Rate of SM decline has been used as a criterion to characterize and filter flash droughts from other nonflash droughts. A common intensification rate-based definition involves decline of RZSM from 40th percentile to below the 20th percentile, with an average decline rate of no less than the fifth percentile for each pentad (Qing et al., 2022; Yuan et al., 2019). Due to the limited availability of SMAP SM observations to calculate percentiles, we analyze the variations in slope of the standardized anomalies of RZSM and LAI at a pentad (5 day) time scale across the different DA and OL (without DA) configurations. The slopes are calculated only over the selected domain (see Figure 1a) which is representative of the affected region common to both the droughts during their onsets. Regions without any drought impact are assumed to be absent during the period of analysis which begins from the last pentad with a positive slope of RZSM (pentad zero) before the decline to pentad with lowest (largest negative) slope. The period extends over the next 1 month (six pentads) after dropping to a negative RZSM slope. Pentad slopes represent the rate of change in landscape and vegetation conditions, often leading to changes in water cycle enough to trigger the flash drought. In fact, the rapid intensification rate is a major contributor to the harm caused to the agricultural industry, where it limits the time for mitigating measures such as additional irrigation arrangements, or delaying the seeding of crops (Hoffman et al., 2021).

Figure 8 shows pentad scale slopes of RZSM and LAI during seven pentads starting from the pentads of 1 May 2016 and 26 April 2017 for the flash droughts of 2016 and 2017 respectively. RZSM slope drops to minimum during the fourth and third pentad for the 2016 and 2017 droughts, respectively. For the 2016 flash drought,

Table 1
Comparison of Weekly Averaged RZSM Anomalies With Reference Data Sets of ESI (Four-Week Composite Product) and Monthly Median USDM Drought Categories, Averaged Over the Months of May-August During the Two Flash Droughts of 2016 and 2017

Year	Reference	Metric	Multi-DA	LAI-DA	SM-DA	OL
2016	ESI	MI score	1.04	0.86	0.81	0.80
	ESI	Pearson's R	0.72	0.71	0.53	0.62
	USDm	F1-score	0.21	0.24	0.20	0.19
	USDm	SSIM	0.49	0.57	0.47	0.51
2017	ESI	MI score	1.11	1.03	1.11	1.04
	ESI	Pearson's R	0.70	0.64	0.69	0.66
	USDm	F1-score	0.27	0.20	0.29	0.20
	USDm	SSIM	0.36	0.29	0.32	0.28

Note. Comparison with USDm is performed using spatial similarity measures of F1-score and Structural Similarity Index (SSIM). Bold indicates the model with the best performance compared to reference data set (ESI/USDm).

LAI-DA captures the rapid rate of decline in RZSM with largest negative slopes at the onset, as high as 10.0% steeper compared to results from OL (Figure 8a). Given the decline in RZSM is driven by high temperatures and increased vegetation transpiration, assimilating vegetation conditions from MODIS LAI improves the ability to model rapid changes in soil dryness. Further, Multi-DA is also able to capture the rapid decline in LAI as a result of increased vegetation stress (Figure 8b). The large difference in slopes between LAI-DA and Multi-DA simulations in the initial couple of pentads is also a result of preceding differences in LAI anomalies during April (see Section 3.2) caused by large spells of precipitation where Multi-DA better captures the reduced stress on vegetation by including both LAI and SM observations. It should also be noted that the decline in LAI, caused by excessive heat and evaporative demands, precedes RZSM drawdown, which again corroborates the warm (heat wave-driven) mechanism of the 2016 flash drought.

During the 2017 drought, in contrast, SM-DA and Multi-DA result in larger negative RZSM slopes over the seven pentads analyzed here (Figure 8c). This rapid rate of initial RZSM decline due to anomalous precipitation was the key factor that led to flash drought in the region. SM-DA resulted in the largest rates of decline in RZSM, as large as 48.4% during the pentad of maximum decline, compared to results from OL. The drier soils thus cause a subsequent

stress on vegetation captured by large negative LAI slopes from Multi-DA over the later pentads (Figure 8d). This follows with a decline in LAI in contrast to the 2016 drought, where drying of soils is an after-effect rather than the cause. The similar slopes of LAI anomalies between Multi-DA and LAI-DA again result from the dry (precipitation deficit-driven) mechanism, where vegetation stress is not the primary driver of drought onset or intensification, in contrast to the 2016 warm flash drought. Thus, assimilating SM observations in the Multi-DA configuration do not have any significant impact on the modeled LAI.

3.5. Multivariate DA Captures Spatial Signatures of Flash Drought Progression

We analyze spatial signatures of RZSM anomalies and vegetation stress indicators to provide a basis for assessing the impact of DA in capturing drought progression and severity. Because of the lack of independent drought reference data, we perform quantitative evaluation of the driving mechanism of the droughts by comparing against common indicators of drought stress and existing drought indices. We first evaluate modeled RZSM anomalies with ESI, which is an indicator of vegetation stress that also responds to changes in SM (Zhong et al., 2020). Table 1 shows MI score), and Pearson's correlation (R) between weekly ESI and RZSM anomalies obtained from OL and DA experiments averaged over May-August. MI score is a measure of similarity between two time series, where a score of zero denotes no similarity (Equation 2). Two-tailed p -value is obtained for testing the significance of correlation between SM and ESI anomalies.

The assessment highlights the different roles of assimilating observations of SM and LAI during various stages of flash drought development. For the 2016 case driven by heat wave, the vegetation pathway drives drought propagation, subsequently modulating SM stress. As a result, only the DA runs that incorporate vegetation information (LAI-DA and Multi-DA) are able to model vegetation stress as evidenced by higher similarity and correlation of modeled RZSM anomalies with ESI in 2016. An increase of 7.5% in the MI score and 14.5% in correlation is obtained using LAI-DA compared to the OL-modeled RZSM anomalies. All the correlation values were statistically significant with p -values well under the significance limit.

In contrast, during the dry flash drought of 2017, assimilation of SM is necessary to capture the impact of flash drought on the rapid drying of soils in summer. As RZSM decreases, less energy is needed to evaporate and transpire water, causing canopy temperatures to elevate in comparison with unstressed vegetation under the same atmospheric conditions (Otkin et al., 2013). SM-DA and Multi-DA outputs capture this control of SM on the ESI during drought intensification, each with a 6.7% increase in MI scores over OL outputs (Table 1).

Table 2
Comparison of Average RMSE and Bias Between LIS-Modeled Surface SM Using Different DA Configurations and USCRN Stations Over the Period of Analysis (Combined Over 2016 and 2017 Drought Periods)

Metric	USCRN station name	Multi-DA	SM-DA	LAI-DA	OL
RMSE	ND_Medora_7_E	0.060	0.060	0.056	0.053
	* SD_Buffalo_13_ESE	0.085	0.085	0.096	0.095
	* WY_Sundance_8_NNW	0.093	0.094	0.114	0.110
	SD_Pierre_24_S	0.108	0.109	0.106	0.106
Bias	ND_Medora_7_E	0.013	0.013	0.026	0.012
	SD_Buffalo_13_ESE	-0.059	-0.059	-0.054	-0.060
	* WY_Sundance_8_NNW	-0.026	-0.026	-0.025	-0.030
	SD_Pierre_24_S	-0.089	-0.090	-0.089	-0.086

Note. Refer to Figure 1a for USCRN station names and locations. Stations where RMSE or bias of Multi-DA is lower than OL with statistical significance are denoted with asterisk and bold font.

Next, to evaluate the DA outputs in terms of their ability to capture the spatial patterns of drought progression, we compared the spatial similarity of RZSM anomalies with the monthly median of weekly USDM drought categories. We used the SSIM (see Equation 3) as a measure of perceived similarity in the spatial distributions of two data sets, varying between zero and one (Wang et al., 2004). Table 1 summarizes average SSIM over the selected domain during May-Aug. Because of the discrete nature of USDM maps, we also calculate another measure of similarity, F1-score, which discretizes the RZSM anomalies to compare against USDM drought categories. Note also that USDM, being a subjective index that relies on a rotating team of authors (Svoboda et al., 2002), may not reliably provide true measures of physical processes. Nevertheless, we use it here as a reference in the absence of other drought information. Highest SSIM of 0.57 (0.36) is obtained with LAI-DA (Multi-DA), an increase of 11.7% (28.6%) over results from OL, for the 2016 (2017) flash droughts. During 2016, RZSM anomalies from Multi-DA entail spatial patterns from both the assimilated variables resulting in lower SSIM values compared to LAI-DA. F1-scores also show similar trends, with an increase of 26.3% (45.0%) from LAI-DA (SM-DA) over results from OL for the 2016 (2017) flash droughts. This again corroborates the role of assimilating LAI (SM) observations in capturing the progression of warm (dry) flash droughts.

The modeled-SM evaluation against USCRN sites is shown in Table 2. Comparison metrics indicate that assimilation of SM and vegetation is generally beneficial as RMSE from Multi-DA has a statistically significant improvement in RMSE at two of the four stations, along with marginal degradations in the other two sites. Since the limited set of in situ stations could be in heterogeneous locations that are difficult to model, they are not enough to provide a fair evaluation of the spatially distributed features of drought evolution. It should also be noted that a large part of the RMSE is due to bias at most of these stations. Nevertheless, the advantage of SM-DA and LAI-DA on the land surface process variables is well established in prior studies (Albergel et al., 2010; Kolassa et al., 2017; Kumar et al., 2014, 2019; Lievens et al., 2017; Liu et al., 2011; Xu et al., 2021).

4. Summary and Conclusions

Soil and vegetation conditions evolve rapidly during the development and intensification of flash droughts. Due to the interactions between the biosphere and hydrosphere, as well as anthropogenic changes, SM and vegetation are critical aspects of the water budget and variability of water cycle components. Assimilation of such observations within LSMs provides a way to model the agricultural and ecological impacts of flash droughts as reflected by changes in the different indicators of droughts. This study provides confirmation of the utility of assimilating SM from downscaled-SMAP product and MODIS-derived LAI retrievals to capture flash drought progression and intensification by improving the LSM estimates. We have also demonstrated which observations are most critical at different stages of flash droughts based on the driving physical mechanism.

The multivariate assimilation is found to benefit 2016 and 2017 flash droughts in distinct ways. During the warm flash drought of 2016 intensified by heat waves at the onset, assimilation of LAI helps the model resolve high transpiration in late spring followed by highly stressed vegetation, which is otherwise not captured by OL and

SM-DA simulations. OL outputs marginally captured some of the drought stages, in part due to the high-quality precipitation inputs from GPM IMERG used to force the Noah-MP model. However, states such as anomalously dry soil conditions or stressed vegetation during droughts are often missing in OL outputs.

The dry flash drought of 2017, however, followed a different mechanism where lack of precipitation drove the reductions in SM, caused higher vegetation stress and negative LAI anomalies. SM-DA is essential to improve the representation of SM conditions and capture the fast rate of decline. The dry conditions, combined with warmer-than-normal temperatures led to a cascade of disturbances that impacted vegetation and sparked various wildfires across the Northern Great Plains.

We also demonstrated the ability to successfully capture the rapid rate of RZSM decline and vegetation deterioration by assimilating the variables that contribute to the onset. This analysis has multiple implications for flash drought monitoring, risk assessment, and in designing effective mitigation strategies. An early indication of rapid change in water availability in the landscape provides early warning and ample window of response to prepare for and minimize consequences of the impending drought risk to the agricultural industry. While near real-time (NRT) drought monitoring is not the focus of this study, the multivariate DA framework of remote sensing observations is also conducive to augment existing NRT monitoring and early warning capabilities, given that most monitoring efforts rely on indices based on observational or reanalysis data sets. MODIS LAI is an 8-day product which is smoothed to daily time scale for DA while SMAP SM is available in near real-time (though in this study we used the SMAP product with a latency of 2 days). The framework can not only improve the predictions of common flash drought indicators, but also provide a holistic understanding of the flashiness, intensification, and evolution of soil and vegetation stresses in flash droughts following different mechanisms (warm or dry).

Comparison of RZSM anomalies with ESI and USDM drought categories further explain the role of multivariate DA. The control of SM on ESI was well-captured by assimilating LAI (SM) observations for warm (dry) flash droughts. In both droughts, negative RZSM anomalies capture early drying of soils and the respective hotspots in the USDM maps, demonstrating another advantage of DA in capturing rapid changes during flash droughts. A comparison is performed to assess the spatial consistency of modeled drought drivers with respect to USDM patterns. However, a more thorough investigation is needed by deriving drought categories from modeled surface and RZSM using the corresponding percentiles used by USDM; the short period of SMAP available for this study limits our analysis. Uncertainties caused by different land covers and irrigation practices in remote sensing estimates of SM or LAI should also be considered in future efforts.

This study emphasizes the need to incorporate multiple observational constraints from remote sensing for capturing the rapid onset rates of the 2016 and 2017 flash droughts and representing their propagation mechanisms and severity. It is noteworthy to mention that while the drivers of 2016 and 2017 droughts have been defined in the literature, in a general case, a-priori knowledge of the drought drivers is absent. Our framework to assimilate different ground observations to model soil and vegetation dynamics is, therefore, a viable approach to capture flash droughts at the required time scale. Further, our characterization of warm versus dry flash droughts, giving more weight to the mechanism that drives the rapid onset rates, help better identify the impact of droughts without being constrained by the duration of anomalous conditions. As such, the 2016 warm flash drought persisted much after the heat waves receded.

Another novel contribution of this study is the improvement in representation of the onset and intensification stages of the two contrasting flash droughts because of simultaneously assimilating SM and LAI conditions. These contributions can be attributed to the distinct impacts of moisture deficits and heat waves on the water cycle. The former evolves because of the anomalous precipitation deficits and rapidly depleted SM moving the landscape into moisture-limited state, which is captured by assimilating information on RZSM. Amplification of warm air temperatures by feedback from the increased sensible heat flux further intensifies drought and stresses vegetation. The latter, however, impacts transpiration at the onset due to high air temperatures and elevated evaporative demands where LAI-DA adds modeling improvements to the vegetation state. Multivariate assimilation thus leverages the advantages of both in improving the representation of key land surface processes that drive and intensify flash droughts.

A relevant issue in flash drought monitoring that needs consideration is the ability of LSMs to represent the rapid time scales involved in these extreme events. Because of the rapid change in water availability associated with a flash drought, the model needs to capture those changes as well as the rate of change in SM conditions,

evaporative demands, and vegetation response at a smaller time scale. The results of this study suggest that assimilation of remotely sensed information within LSMs from products with finer temporal resolution provides a practical approach for improving the characterization, even when the model physics is not fully adequate to represent the complex underlying processes and their interactions.

Flash droughts significantly impact crops and ecology due to their rapid development allowing a very small window to respond and plan mitigation strategies. The study has broader implications for flash drought characterization by demonstrating the utility of combined use of models and multiple remote sensing sources in promoting proactive risk management strategies resilient to hydrologic extremes.

Data Availability Statement

Various data sets used in this study are available from the following websites: SMAP Soil Moisture—<https://nsidc.org/data/smap/smap-data.html>; MCD15A2H—<https://lpdaac.usgs.gov/products/mcd15a2hv006/>; ESI—<https://gis1.serviglobal.net/data/esi/>; and USDM—<https://droughtmonitor.unl.edu/DmData/DataDownload.aspx>.

References

- Albergel, C., Calvet, J. C., Mahfouf, J. F., Rüdiger, C., Barbu, A. L., Lafont, S., et al. (2010). Monitoring of water and carbon fluxes using a land data assimilation system: A case study for southwestern France. *Hydrology and Earth System Sciences*, *14*(6), 1109–1124. <https://doi.org/10.5194/hess-14-1109-2010>
- Anderson, M. C., Hain, C., Wardlow, B., Pimstein, A., Mecikalski, J. R., & Kustas, W. P. (2011). Evaluation of drought indices based on thermal remote sensing of evapotranspiration over the continental United States. *Journal of Climate*, *24*(8), 2025–2044. <https://doi.org/10.1175/2010jcli3812.1>
- Anderson, M. C., Norman, J. M., Mecikalski, J. R., Otkin, J. A., & Kustas, W. P. (2007). A climatological study of evapotranspiration and moisture stress across the continental United States based on thermal remote sensing: II. Surface moisture climatology. *Journal of Geophysical Research*, *112*, D10117. <https://doi.org/10.1029/2006JD007507>
- Basara, J. B., Christian, J. I., Wakefield, R. A., Otkin, J. A., Hunt, E. H., & Brown, D. P. (2019). The evolution, propagation, and spread of flash drought in the Central United States during 2012. *Environmental Research Letters*, *14*(8), 084025. <https://doi.org/10.1088/1748-9326/ab2cc0>
- Bolten, J. D., Crow, W. T., Zhan, X., Jackson, T. J., & Reynolds, C. A. (2009). Evaluating the utility of remotely sensed soil moisture retrievals for operational agricultural drought monitoring. *IEEE Journal of Selected Topics in Applied Earth Observations and Remote Sensing*, *3*(1), 57–66.
- Christian, J. I., Basara, J. B., Hunt, E. D., Otkin, J. A., Furtado, J. C., Mishra, V., et al. (2021). Global distribution, trends, and drivers of flash drought occurrence. *Nature Communications*, *12*(1), 6330. <https://doi.org/10.1038/s41467-021-26692-z>
- Christian, J. I., Basara, J. B., Otkin, J. A., Hunt, E. D., Wakefield, R. A., Flanagan, P. X., & Xiao, X. (2019). A methodology for flash drought identification: Application of flash drought frequency across the United States. *Journal of Hydrometeorology*, *20*(5), 833–846. <https://doi.org/10.1175/jhm-d-18-0198.1>
- Entekhabi, D., Njoku, E. G., O'Neill, P. E., Kellogg, K. H., Crow, W. T., Edelstein, W. N., et al. (2010). The soil moisture active passive (SMAP) mission. *Proceedings of the IEEE*, *98*(5), 704–716.
- Ford, T. W., & Labosier, C. F. (2017). Meteorological conditions associated with the onset of flash drought in the eastern United States. *Agricultural and Forest Meteorology*, *247*, 414–423. <https://doi.org/10.1016/j.agrformet.2017.08.031>
- Gavahi, K., Abbaszadeh, P., Moradkhani, H., Zhan, X., & Hain, C. (2020). Multivariate assimilation of remotely sensed soil moisture and evapotranspiration for drought monitoring. *Journal of Hydrometeorology*, *21*(10), 2293–2308. <https://doi.org/10.1175/jhm-d-20-0057.1>
- Gelaro, R., McCarty, W., Suárez, M. J., Todling, R., Molod, A., Takacs, L., et al. (2017). The Modern-Era Retrospective Analysis for Research and Applications, Version 2 (MERRA-2). *Journal of Climate*, *30*(14), 5419–5454. <https://doi.org/10.1175/jcli-d-16-0758.1>
- Gerken, T., Bromley, G. T., Ruddell, B. L., Williams, S., & Stoy, P. C. (2018). Convective suppression before and during the United States Northern Great Plains flash drought of 2017. *Hydrology and Earth System Sciences*, *22*(8), 4155–4163. <https://doi.org/10.5194/hess-22-4155-2018>
- He, M., Kimball, J. S., Yi, Y., Running, S., Guan, K., Jencso, K., et al. (2019). Impacts of the 2017 flash drought in the US Northern plains informed by satellite-based evapotranspiration and solar-induced fluorescence. *Environmental Research Letters*, *14*(7), 074019. <https://doi.org/10.1088/1748-9326/ab22c3>
- Hobbins, M. T., Wood, A., McEvoy, D. J., Huntington, J. L., Morton, C., Anderson, M., & Hain, C. (2016). The evaporative demand drought index. Part I: Linking drought evolution to variations in evaporative demand. *Journal of Hydrometeorology*, *17*(6), 1745–1761. <https://doi.org/10.1175/jhm-d-15-0121.1>
- Hoell, A., Perlwitz, J., & Eischeid, J. K. (2019). The causes, predictability, and historical context of the 2017 US Northern Great Plains drought (p. 25). Retrieved from <https://repository.library.noaa.gov/view/noaa/23003>
- Hoffmann, D., Gallant, A. J., & Hobbins, M. (2021). Flash drought in CMIP5 models. *Journal of Hydrometeorology*, *22*(6), 1439–1454. <https://doi.org/10.1175/jhm-d-20-0262.1>
- Huffman, G. J., Bolvin, D. T., Braithwaite, D., Hsu, K., Joyce, R., Xie, P., & Yoo, S. H. (2015). NASA global precipitation measurement (GPM) integrated multi-satellite retrievals for GPM (IMERG). *Algorithm Theoretical Basis Document (ATBD) Version, 4* (p. 26).
- Jencso, K., Parker, B., Downey, M., Hadwen, T., Howell, A., Leaf, J. R., et al. (2019). *Flash drought: Lessons learned from the 2017 drought across the US Northern Plains and Canadian Prairies*. NOAA National Integrated Drought Information System.
- Kimball, J. S., Jones, L., Jencso, K., He, M., Maneta, M., & Reichle, R. (2019). SMAP L4 assessment of the US Northern Plains 2017 flash drought. In *IEEE International Geoscience and Remote Sensing Symposium* (pp. 5366–5369).
- Kolassa, J., Reichle, R. H., & Draper, C. S. (2017). Merging active and passive microwave observations in soil moisture data assimilation. *Remote Sensing of Environment*, *191*, 117–130. <https://doi.org/10.1016/j.rse.2017.01.015>
- Kumar, S. V., Holmes, T., Andela, N., Dharssi, I., Hain, C., Peters-Lidard, C., et al. (2021). The 2019–2020 Australian drought and bushfires altered the partitioning of hydrological fluxes. *Geophysical Research Letters*, *48*, e2020GL091411. <https://doi.org/10.1029/2020GL091411>

- Kumar, S. V., Jasinski, M., Mocko, D. M., Rodell, M., Borak, J., Li, B., et al. (2019). NCA-LDAS land analysis: Development and performance of a multisensor, multivariate land data assimilation system for the National Climate Assessment. *Journal of Hydrometeorology*, *20*(8), 1571–1593. <https://doi.org/10.1175/jhm-d-17-0125.1>
- Kumar, S. V., Mocko, D. M., Wang, S., Peters-Lidard, C. D., & Borak, J. (2019). Assimilation of remotely sensed leaf area index into the Noah-MP land surface model: Impacts on water and carbon fluxes and states over the continental United States. *Journal of Hydrometeorology*, *20*(7), 1359–1377. <https://doi.org/10.1175/jhm-d-18-0237.1>
- Kumar, S. V., Peters-Lidard, C. D., Mocko, D., Reichle, R., Liu, Y., Arsenault, K. R., et al. (2014). Assimilation of remotely sensed soil moisture and snow depth retrievals for drought estimation. *Journal of Hydrometeorology*, *15*(6), 2446–2469. <https://doi.org/10.1175/jhm-d-13-0132.1>
- Kumar, S. V., Peters-Lidard, C. D., Tian, Y., Houser, P. R., Geiger, J., Olden, S., et al. (2006). Land information system: An interoperable framework for high resolution land surface modeling. *Environmental Modelling & Software*, *21*(10), 1402–1415. <https://doi.org/10.1016/j.envsoft.2005.07.004>
- Kumar, S. V., Reichle, R. H., Koster, R. D., Crow, W. T., & Peters-Lidard, C. D. (2009). Role of subsurface physics in the assimilation of surface soil moisture observations. *Journal of Hydrometeorology*, *10*(6), 1534–1547.
- Lievens, H., Reichle, R. H., Liu, Q., De Lannoy, G. J., Dunbar, R. S., Kim, S. B., et al. (2017). Joint Sentinel-1 and SMAP data assimilation to improve soil moisture estimates. *Geophysical Research Letters*, *44*, 6145–6153. <https://doi.org/10.1002/2017GL073904>
- Lisonbee, J., Woloszyn, M., & Skumanich, M. (2021). Making sense of flash drought: Definitions, indicators, and where we go from here. *Journal of Applied and Service Climatology*, *2021*, 1–19.
- Liu, P. W., Bindlish, R., Fang, B., Lakshmi, V., O'Neill, P. E., Yang, Z., et al. (2021). Assessing disaggregated SMAP soil moisture products in the United States. *IEEE Journal of Selected Topics in Applied Earth Observations and Remote Sensing*, *14*, 2577–2592.
- Liu, P. W., Bindlish, R., O'Neill, P. E., Fang, B., Lakshmi, V., Yang, Z., et al. (2022). Thermal hydraulic disaggregation of SMAP soil moisture over the continental United States. *IEEE Journal of Selected Topics in Applied Earth Observations and Remote Sensing*, *15*, 4072–4093. <https://doi.org/10.1109/JSTARS.2022.3165644>
- Liu, Q., Reichle, R. H., Bindlish, R., Cosh, M. H., Crow, W. T., de Jeu, R., et al. (2011). The contributions of precipitation and soil moisture observations to the skill of soil moisture estimates in a land data assimilation system. *Journal of Hydrometeorology*, *12*(5), 750–765.
- Liu, X., Li, Z., & Attarod, P. (2021). Understanding hydrological extremes and their impact in a changing climate: Observations, modeling and attribution. *Frontiers of Earth Science*, *8*, 657.
- Liu, Y., Peters-Lidard, C. D., Kumar, S., Foster, J. L., Shaw, M., Tian, Y., & Fall, G. M. (2013). Assimilating satellite-based snow depth and snow cover products for improving snow predictions in Alaska. *Advances in Water Resources*, *54*, 208–227.
- Liu, Y., Peters-Lidard, C. D., Kumar, S. V., Arsenault, K. R., & Mocko, D. M. (2015). Blending satellite-based snow depth products with in situ observations for streamflow predictions in the Upper Colorado River Basin. *Water Resources Research*, *51*, 1182–1202. <https://doi.org/10.1002/2014WR016606>
- Mishra, V., Aadhar, S., & Mahto, S. S. (2021). Anthropogenic warming and intraseasonal summer monsoon variability amplify the risk of future flash droughts in India. *npj Climate and Atmospheric Science*, *4*(1), 1–10.
- Mladenova, I. E., Bolten, J. D., Crow, W. T., Sazib, N., Cosh, M. H., Tucker, C. J., & Reynolds, C. (2019). Evaluating the operational application of SMAP for global agricultural drought monitoring. *IEEE Journal of Selected Topics in Applied Earth Observations and Remote Sensing*, *12*(9), 3387–3397.
- Mo, K. C., & Lettenmaier, D. P. (2016). Precipitation deficit flash droughts over the United States. *Journal of Hydrometeorology*, *17*(4), 1169–1184.
- Mocko, D. M., Kumar, S. V., Peters-Lidard, C. D., & Wang, S. (2021). Assimilation of vegetation conditions improves the representation of drought over agricultural areas. *Journal of Hydrometeorology*, *22*(5), 1085–1098.
- Mozny, M., Trnka, M., Zalud, Z., Hlavinka, P., Nekoar, J., Potop, V., & Virag, M. (2012). Use of a soil moisture network for drought monitoring in the Czech Republic. *Theoretical and Applied Climatology*, *107*(1), 99–111.
- Myneni, R., Knyazikhin, Y., & Park, T. (2015). MCD15A2H MODIS/Terra+Aqua Leaf Area Index/FPAR 8-day L4 Global 500m SIN Grid V006. [Dataset]. NASA EOSDIS Land Processes DAAC. <https://lpdaac.usgs.gov/products/mcd15a2hv006/>
- Nie, W., Kumar, S. V., Arsenault, K. R., Peters-Lidard, C. D., Mladenova, I. E., Bergaoui, K., et al. (2021). Towards effective drought monitoring in the Middle East and North Africa (MENA) region: Implications from assimilating leaf area index and soil moisture into the Noah-MP land surface model for Morocco. *Hydrology and Earth System Sciences Discussions*, *26*, 2365–2386.
- Niu, G. Y., Yang, Z. L., Mitchell, K. E., Chen, F., Ek, M. B., Barlage, M., et al. (2011). The community Noah land surface model with multiparameterization options (Noah-MP): I. Model description and evaluation with local-scale measurements. *Journal of Geophysical Research*, *116*, D12109. <https://doi.org/10.1029/2010JD015139>
- Otkin, J. A., Anderson, M. C., Hain, C., Mladenova, I. E., Basara, J. B., & Svoboda, M. (2013). Examining rapid onset drought development using the thermal infrared-based evaporative stress index. *Journal of Hydrometeorology*, *14*(4), 1057–1074.
- Otkin, J. A., Haigh, T., Mucia, A., Anderson, M. C., & Hain, C. (2018b). Comparison of agricultural stakeholder survey results and drought monitoring datasets during the 2016 US Northern Plains flash drought. *Weather, Climate, and Society*, *10*(4), 867–883.
- Otkin, J. A., Svoboda, M., Hunt, E. D., Ford, T. W., Anderson, M. C., Hain, C., & Basara, J. B. (2018). Flash droughts: A review and assessment of the challenges imposed by rapid-onset droughts in the United States. *Bulletin of the American Meteorological Society*, *99*(5), 911–919.
- Otkin, J. A., Zhong, Y., Hunt, E. D., Basara, J., Svoboda, M., Anderson, M. C., & Hain, C. (2019). Assessing the evolution of soil moisture and vegetation conditions during a flash drought-flash recovery sequence over the South-Central United States. *Journal of Hydrometeorology*, *20*(3), 549–562.
- Pendergrass, A. G., Meehl, G. A., Pulwarty, R., Hobbins, M., Hoell, A., AghaKouchak, A., et al. (2020). Flash droughts present a new challenge for subseasonal-to-seasonal prediction. *Nature Climate Change*, *10*(3), 191–199.
- Qing, Y., Wang, S., Ancell, B. C., & Yang, Z. L. (2022). Accelerating flash droughts induced by the joint influence of soil moisture depletion and atmospheric aridity. *Nature Communications*, *13*(1), 1139.
- Reichle, R. H., McLaughlin, D. B., & Entekhabi, D. (2002). Hydrologic data assimilation with the ensemble Kalman filter. *Monthly Weather Review*, *130*(1), 103–114.
- Samaniego, L., Thober, S., Kumar, R., Wanders, N., Rakovec, O., Pan, M., et al. (2018). Anthropogenic warming exacerbates European soil moisture droughts. *Nature Climate Change*, *8*(5), 421–426.
- Sehgal, V., Gaur, N., & Mohanty, B. P. (2021). Global flash drought monitoring using surface soil moisture. *Water Resources Research*, *57*, e2021WR029901. <https://doi.org/10.1029/2021WR029901>
- Svoboda, M., LeComte, D., Hayes, M., Heim, R., Gleason, K., Angel, J., et al. (2002). The drought monitor. *Bulletin of the American Meteorological Society*, *83*(8), 1181–1190. <https://doi.org/10.1175/1520-0477-83.8.1181>

- Tuttle, S. E., & Salvucci, G. D. (2014). A new approach for validating satellite estimates of soil moisture using large-scale precipitation: Comparing AMSR-E products. *Remote Sensing of Environment*, *142*, 207–222.
- Walker, E., García, G. A., & Venturini, V. (2019). Evapotranspiration estimation using SMAP soil moisture products and bouchet complementary evapotranspiration over Southern Great Plains. *Journal of Arid Environments*, *163*, 34–40. <https://doi.org/10.1016/j.jaridenv.2019.01.002>
- Wang, L., Yuan, X., Xie, Z., Wu, P., & Li, Y. (2016). Increasing flash droughts over China during the recent global warming hiatus. *Scientific Reports*, *6*(1), 30571.
- Wang, Z., Bovik, A. C., Sheikh, H. R., & Simoncelli, E. P. (2004). Image quality assessment: From error visibility to structural similarity. *IEEE Transactions on Image Processing*, *13*(4), 600–612.
- Wilhite, D. A., & Glantz, M. H. (1985). Understanding the drought phenomenon: The role of definitions. *Water International*, *10*(3), 111–120.
- Woloszyn, M., Skumanich, M., Lisonbee, J., Deheza, V., Hobbins, M., Hoell, A., et al. (2021). *Flash drought: Current understanding and future priorities; report of the 2020 NIDIS flash drought virtual workshop*. NOAA National Integrated Drought Information System.
- Xu, L., Abbaszadeh, P., Moradkhani, H., Chen, N., & Zhang, X. (2020). Continental drought monitoring using satellite soil moisture, data assimilation and an integrated drought index. *Remote Sensing of Environment*, *250*, 112028.
- Xu, T., Chen, F., He, X., Barlage, M., Zhang, Z., Liu, S., & He, X. (2021). Improve the performance of the Noah-MP-crop model by jointly assimilating soil moisture and vegetation phenology data. *Journal of Advances in Modeling Earth Systems*, *13*, e2020MS002394. <https://doi.org/10.1029/2020MS002394>
- Yan, H., Zarekarizi, M., & Moradkhani, H. (2018). Toward improving drought monitoring using the remotely sensed soil moisture assimilation: A parallel particle filtering framework. *Remote Sensing of Environment*, *216*, 456–471.
- Yang, Z. L., Niu, G. Y., Mitchell, K. E., Chen, F., Ek, M. B., Barlage, M., et al. (2011). The community Noah land surface model with multiparameterization options (Noah-MP): 2. Evaluation over global river basins. *Journal of Geophysical Research*, *116*, D12110. <https://doi.org/10.1029/2010JD015140>
- Yin, J., Zhan, X., Zheng, Y., Liu, J., Fang, L., & Hain, C. R. (2015). Enhancing model skill by assimilating SMOPS blended soil moisture product into Noah land surface model. *Journal of Hydrometeorology*, *16*(2), 917–931.
- Yuan, X., Wang, L., Wu, P., Ji, P., Sheffield, J., & Zhang, M. (2019). Anthropogenic shift towards higher risk of flash drought over China. *Nature Communications*, *10*(1), 4661.
- Zhang, Y., You, Q., Chen, C., & Li, X. (2017). Flash droughts in a typical humid and subtropical basin: A case study in the Gan River Basin, China. *Journal of Hydrology*, *551*, 162–176.
- Zhong, Y., Otkin, J. A., Anderson, M. C., & Hain, C. (2020). Investigating the relationship between the Evaporative Stress Index and land surface conditions in the contiguous United States. *Journal of Hydrometeorology*, *21*(7), 1469–1484.